Innovative Printing Strategy for High-Resolution Jewelry Production by Selective Laser Melting

Damiano Zito, Elia Saccardo,
Dr. Patrizio Sbornicchia, Dr. Valentina Allodi,
Gisela A Cepeda Arque
Progold S.p.A. (Progol3D®)
Trissino (VI), Italy

Introduction

The company history on Selective Laser Melting (SLM) dates back to about a decade ago. Over the course of the years, the research has touched several topics to evaluate the general performance of this recent jewelry manufacturing process, starting from parameter selection to particle-size distribution and flowability to obtain denser items and uniform powder layers.[1,2,3] This was followed by trace additions of semiconductor elements (Ge, Si) to increase the laser absorption as well as changing the structure of the support systems that led to a significant reduction in roughness and residual porosity.[3,4] Other research has compared the traditional lost-wax investment process to selective laser melting in producing typical decorative details or very nice platinum jewelry[5,6] and demonstrated the opportunity of the printing process as a magic pot to produce outstanding hard, white-gold alloys[7] with very unusual elements (Nb, Ti) and that have a milder environmental impact.[8]

The aim of this research was studying how to increase printing resolution to allow the manufacture of jewelry items having very sharp and detailed decorative structures and elements. This advantage would make laser printing not only much more competitive with respect to direct investment casting, but would also allow for producing innovative and complex geometries with larger size, less weight and better mechanical strength. In addition, the greater stability derived from higher resolution could allow a better finish on the jewelry.

Experimental Method

The construction process was performed using an SLM™ printer (SLM-50®) equipped with a 100 W pulsed fiber laser and a 70 mm diameter building platform. The machine maintains an inert gas atmosphere (Ar) during the entire printing process; oxygen content is kept under 0.2% inside the printing chamber. This research used a 750‰ yellow-gold alloy (defined as 2N color, according to ISO 8654:2018) specifically engineered for laser melting processes and produced by gas atomization. The complete process flowchart can be seen in Figure 1. The desiccation process was performed using a vacuum oven for two hours at 250°C/482°F to eliminate as much surface humidity as possible that could hinder

a suitable flowability. The primary coarse sieving was carried out at 53 µm to eliminate the bigger atomized debris and prepare the powder for a subsequent classification at 25 µm.

The particle size distribution after the first classification step was determined by a laser granulometer providing a $d_{90,volume}$ = 21.68 µm (Figure 2). The gold powder also included the smallest fraction of particles; they derive directly from the atomization process and were typically bigger than 500 nm. After classification, the powder had a very good flowability to create a homogenous powder bed after machine recoating (i.e., powder spreading on machine powder bed). Typically, the smaller the particles, the higher the friction will be among them.[2] The high flowability of powders used in this research work was obtained thanks to our company's know-how.

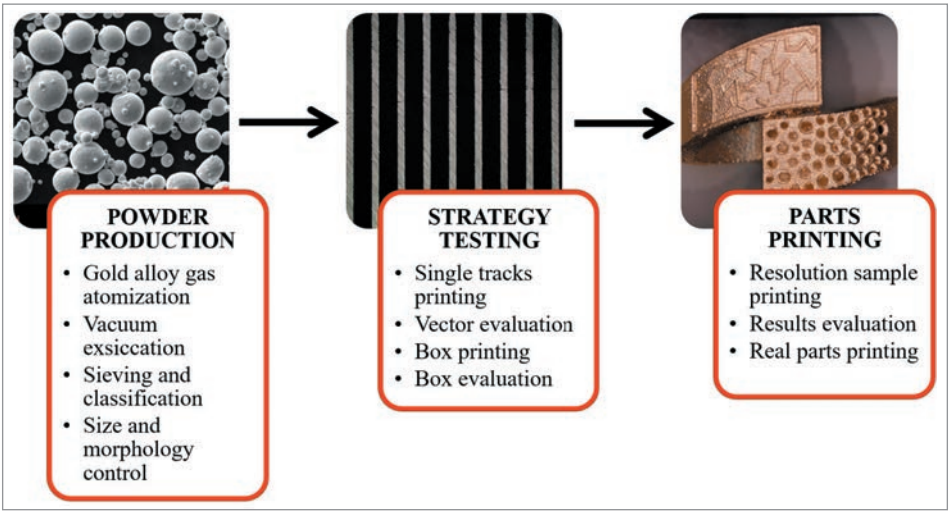

Figure 1 *Overall research flowchart*

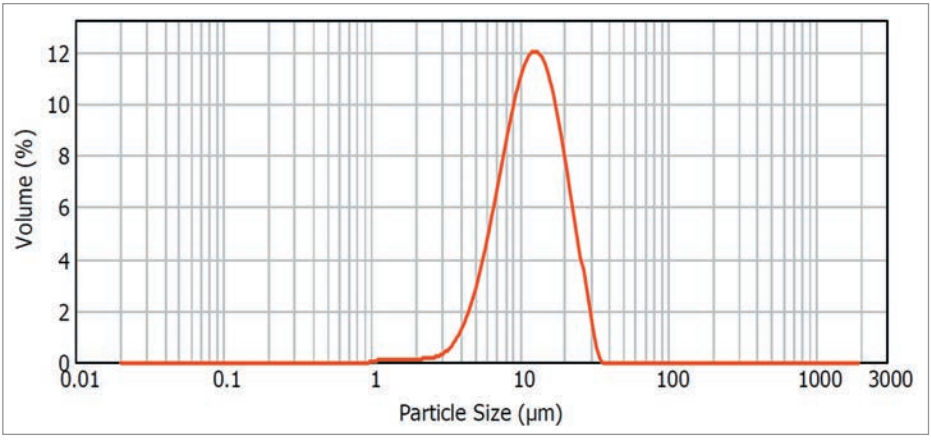

Figure 2 *Particle-size distribution after classification below 25 µm*

The powder morphology was analyzed by electron microscopy (Zeiss, EVO10), which showed spherical particles (Figure 3). In order to check the powder flowability, an avalanche optical flowmeter (Revolution) was used. After executing an initial test with coarser powder (0–25 µm), a second batch was atomized and classified to obtain a finer powder (0–15 µm), which was used not only to build a 30 µm layer in the first case, but also to evaluate 15 µm and 20 µm building layers, always using the same procedure (Table 1). Granulometry of finer powder shows a $d_{90,volume}$ = 15.38 µm (Figures 4 and 5).

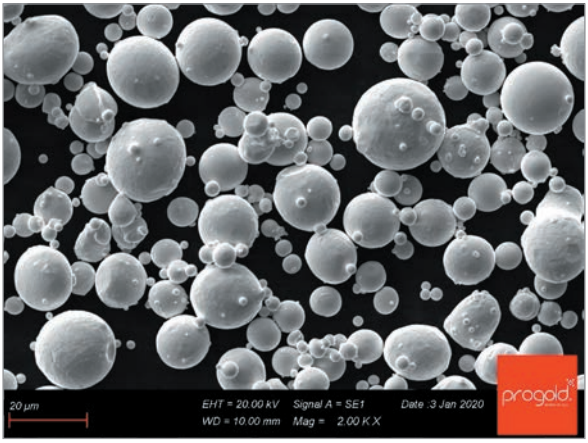

Figure 3 *SEM image of 0–25 µm powder morphology*

Table 1 *General layout for experimental laser conditions*

POWDER SIZE [µm]	BUILDING LAYER [µm]	LASER POWER [W]	EXPOSURE TIME [µs]	SPOT DISTANCE [µm]
0–25	30	9–115	30–200	10–20
0–15	30	19–103	40–200	10–15
	20	13–78	40–200	10–15
	15	25–63	40–200	10–15

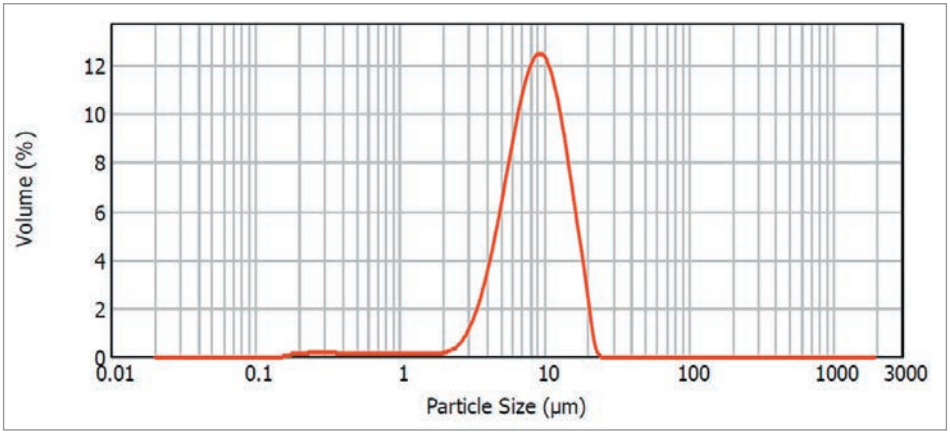

Figure 4 *Particle-size distribution after classification below 15 µm*

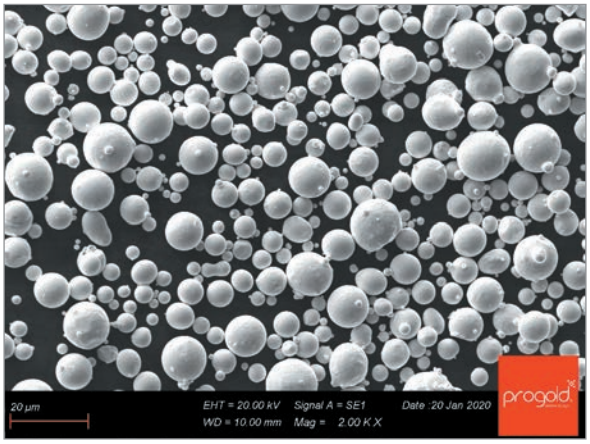

Figure 5 *SEM image of 0–15 µm powder morphology*

In all cases, tests started with printing simple linear vectors. From those results, boxes, resolution samples and roughness samples were printed, as shown in Figure 6. The linear vector tracks were evaluated based on their thickness, continuity and straightness. All tested vectors are reported using graphs: disk diameter corresponds to the thickness of tracks as a function of scanning speed [m/s] and laser power [W]. Good, average or bad vector stability is represented by color: green, yellow and red, respectively (see graph example in Figure 7).

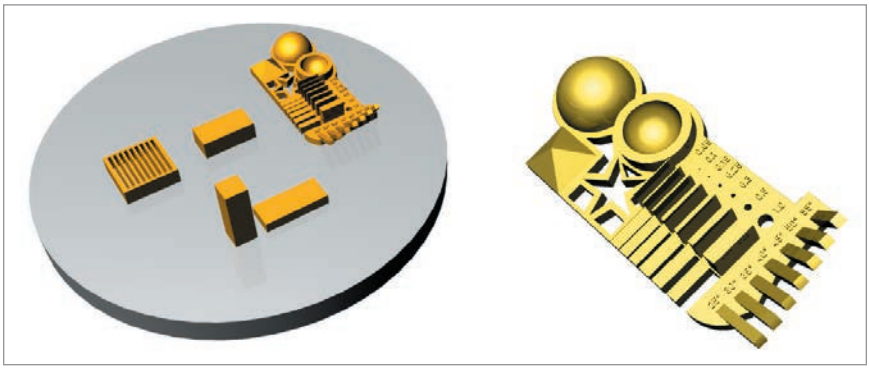

Figure 6 *From the left: vector sample, box, resolution sample and roughness sample; on the right: a digital rendering of resolution sample*

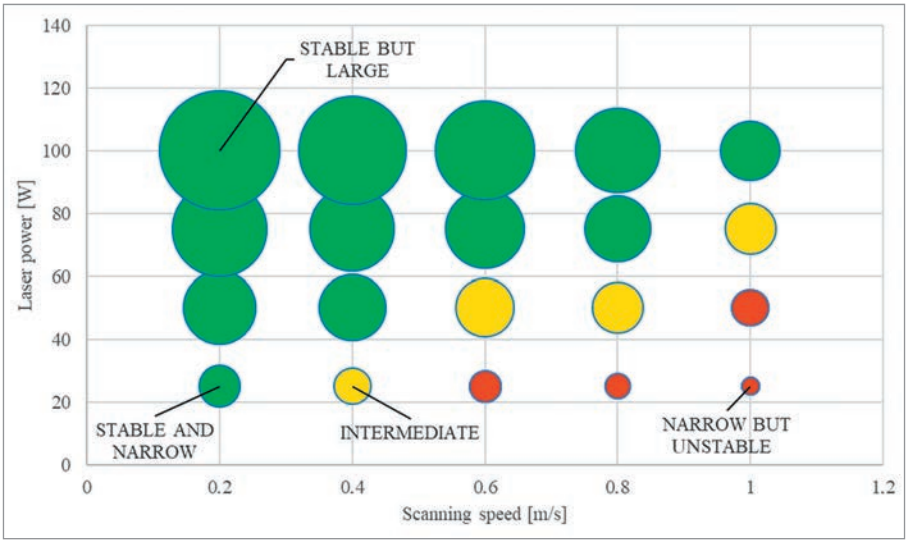

Figure 7 *Example of graph for single tracks*

The trials with gold powder were aimed at finding printing parameters capable of producing the thinnest and most uniform tracks possible using pulsed laser and to obtain the desired increase in resolution. The diagram of laser power as a function of the scanning speed discloses energy regions along which the tracks' melting pool is stable (green), as demonstrated by other authors for different powder materials (INOX 316L).[9] This advantage may also enable finding the narrowest track thickness parameter set; that is the first step to increase printing resolution. The second printing batch (powder 0–15 µm) was primarily divided into three different sets of experiments with layer thicknesses of 30 µm, 20 µm and 15 µm in order to evaluate the possible resolution increase as a function of layer height.

Once a selection of the best laser parameters for single metal tracks was determined, these printing parameters were used to build massive and more realistic specimens. Two kinds of characterization samples were used. The first was a simple prismatic geometry named box to help evaluate the ability of the laser scanning strategy to densify the molten metal stripes. The second was an ensemble of complex-shaped modules, each of them thought to test specific abilities of laser melting for critical geometries such as undercut, slope and detail resolution, which are common in real jewelry manufacturing.

The selection of single-track parameters was done by building stripe-like samples (left sample in Figure 6) as in past research,[3] and progressively changing laser power and laser scan velocity. The evaluation of single tracks was done by optical digital microscopy (VHX, Keyence) on the metallographic section of the samples set into acrylic resins to avoid deformation of metal during polishing. Analogous inspections were made for massive boxes (cut through at half their height) to check the possible presence of internal porosity and cracks. Optical digital microscope and scanning electron microscope (ZEISS EVO 10) were used to evaluate the resolution samples. Roughness samples were measured using a Taylor Hobson® roughness tester (Form Talysurf® 50).

The box printing strategy included different trials in order to enhance the best track parameters obtained in single vectors and to get a dense and constant uniformity in the bulk of box samples. Indeed, the printing process of multiple tracks is very different from the single track because there is a continuous interaction between the massive part already melted and the molten pool beside it. The interaction consists of a faster thermal exchange. Thus, the solidification and densification mechanisms are different, and the danger of residual porosity is increased.

The goal of improving surface quality and detail resolution was studied by using different contouring and hatching strategies. The general layout for laser scanning into a single layer consists of an external thin track named outer, inner large tracks named hatches, and some intermediate tracks named fill lines (Figure 8). Fill lines have the role of filling the space between hatches and the outer shell because hatch tips typically show a roundish shape that could lead to porosity. Hatching is essentially based on a couple of strategies. One is where hatch tracks are simply piled up layer by layer; another consists of shifted hatches between subsequent layers. Shifted hatches mean that the laser scanning of the current layer is performed virtually between the previous layer's hatch tracks. As investigated by Xubin and Yongqiang,[10] the shifted scan strategy should lead to less residual porosity. Inside the single layer, adjacent tracks were overlapped in different percentages, both for piled up tracks and shifted ones. A zero overlapping means no overlap between tracks, whereas a 100% overlapping means that the track is completely scanned over the previous one into the same layer. Usually, the lower the track overlap is, the higher the risk of missing adhesion and porosity between tracks. It is important to note that high overlapping values mean a slower building rate and that a higher portion of the built part is being melted twice. With this perspective, a well-calibrated overlapping must be found to get a fully dense piece. Different tests using various percentages of overlapping resulted in 75% being the best compromise to obtain the best surface quality and to reduce residual porosity.

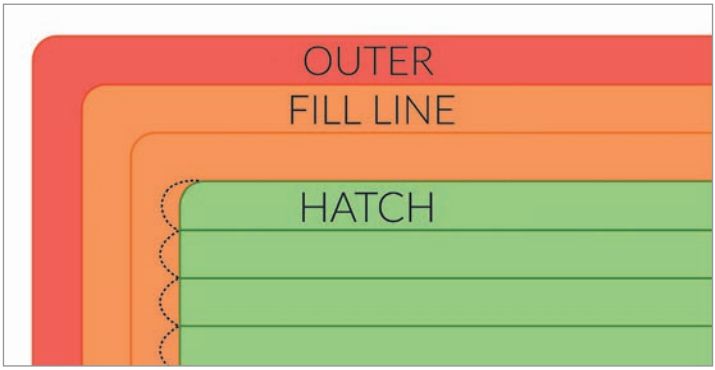

Figure 8 *General scan strategy for a single slice*

Results and Discussion

In order to understand why a thin vector (<100 µm) is needed to increase the resolution, the "beam compensation" parameter should be explained. Beam compensation is a machine parameter that compensates the vector thickness over the digital file contour. When beam compensation is set to 0 mm, the laser will scan exactly on the file contour. As a consequence, the items will be larger than expected since the outer tracks will exceed half of their thickness from the file contour. Figure 9 shows an example of beam compensation at 0 mm. Figure 10 shows a beam compensation equal to the track thickness. By doing this the machine software automatically moves the laser path inward by half of the beam compensation (i.e., outside border of outer vector should coincide with file contour). As can be seen in Figure 10, the laser cannot scan the protrusion on the left because the outer vector thickness is too high and cannot "enter" the thinner protrusion. This is basically the reason why a thin vector under 100 µm is needed to get coherence between file contour and laser path. For this reason, the beam compensation is usually equal to outer vector thickness. Thus, if outer vector is thicker than a file detail, that detail will not be scanned.

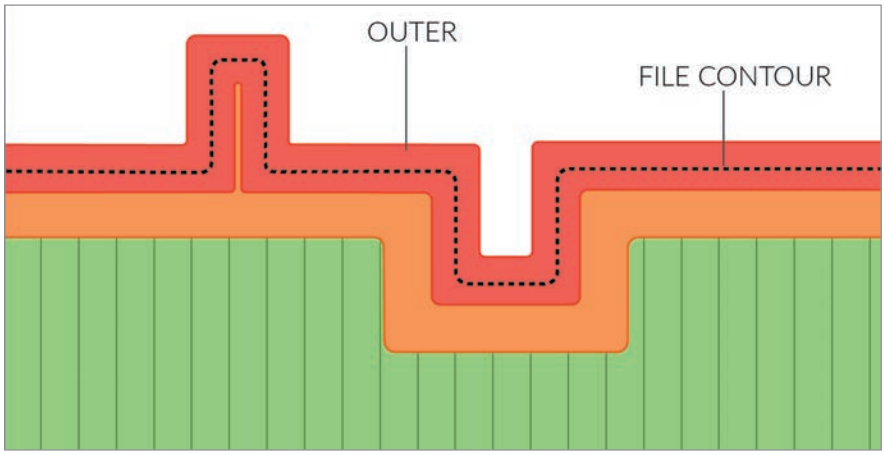

Figure 9 *Graphic representation of laser scan with beam compensation of 0 mm*

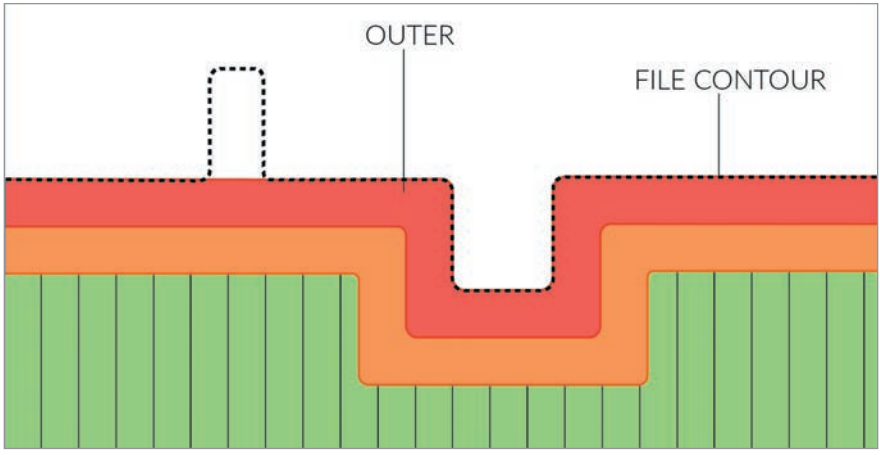

Figure 10 *Graphic representation of laser scan with beam compensation equal to track thickness*

The first building trial (TEST1) started with powder 0–25 µm and layer thickness 30 µm, laser power ranging from about 38 to 65 W and scanning speed between 0.25 and 0.33 m/s (Figure 11). The resulting quality was acceptable only for three samples (S1, S5, S9), but their thickness was quite large (i.e., over 100 µm) and, therefore, not suitable to fulfill the requirements of resolution increase.

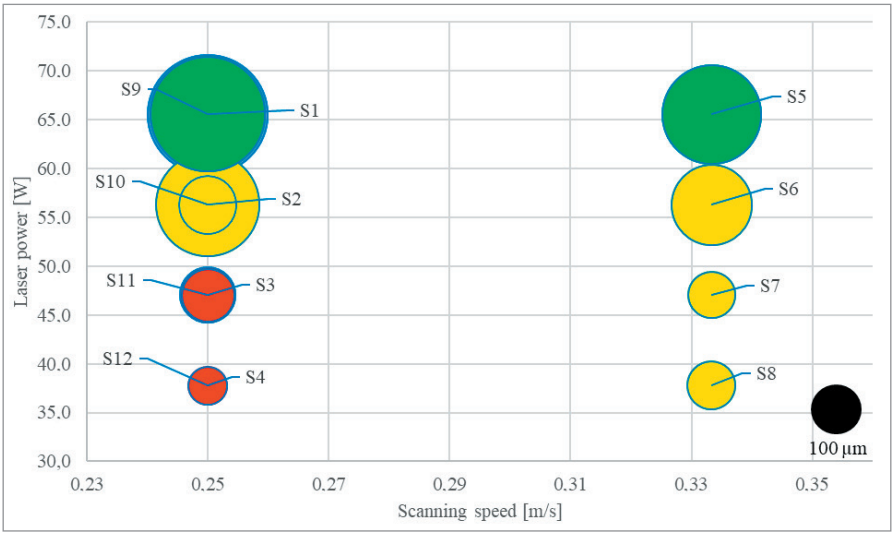

Figure 11 *TEST1 vector results graphically displayed (powder 0–25 µm and layer thickness 30 µm)*

As seen in Figure 11, vectors S9 to S12 are superimposed onto vectors S1 to S4 because they have the same power and scanning speed. This could be explained taking in account the two parameters from which scanning speed derives, namely exposure time [µs] and spot distance traveled [µm]. The scanning speed for a pulsed laser source is calculated as the ratio between spot travel distance and exposure time. In TEST1, for example, vectors S1–S4 have exposure time of 40 µs and spot distance of 10 µm; vectors S9–S12 have exposure time of 60 µs and spot distance of 15 µm. The result is that they both have a scanning speed equal to 0.25 m/s.

TEST2 was performed using laser power ranging from about 20 to 56 W and scanning speed ranging from 0.17 to 0.375 m/s (Figure 12). In this test the only track (S8) with acceptable quality is bigger than the reference target limit (≈100 µm) for improving surface resolution. There are a similar number of tracks with average uniformity (yellow colored).

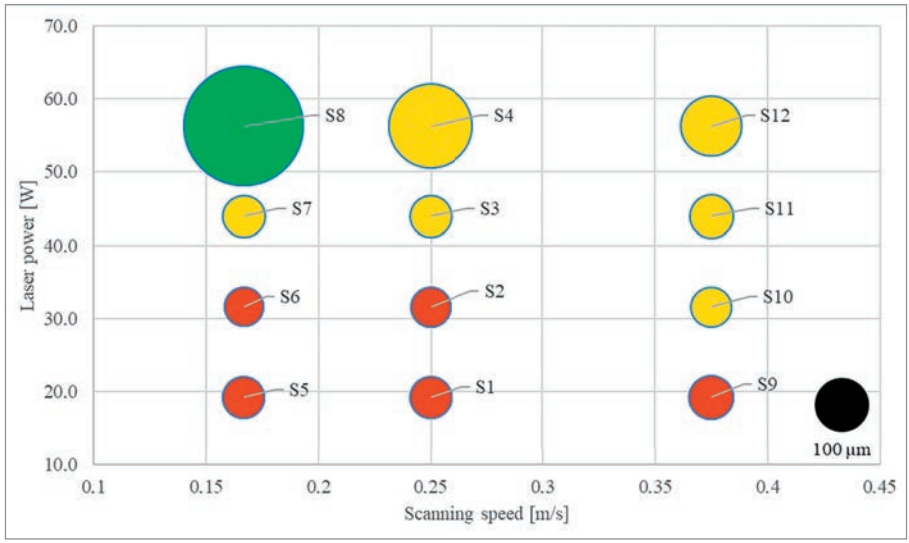

Figure 12 *TEST2 tracks thickness and quality for powder 0–25 µm and layer thickness 30 µm*

In TEST3, building trials showed an increase of acceptable vectors (S4, S5, S8, S9, S10), but their width is still large, 230–370 µm (Figure 13). The thinner tracks were still too rough either due to balling effect[9] or to the instability of the melting pool because of insufficient energy.

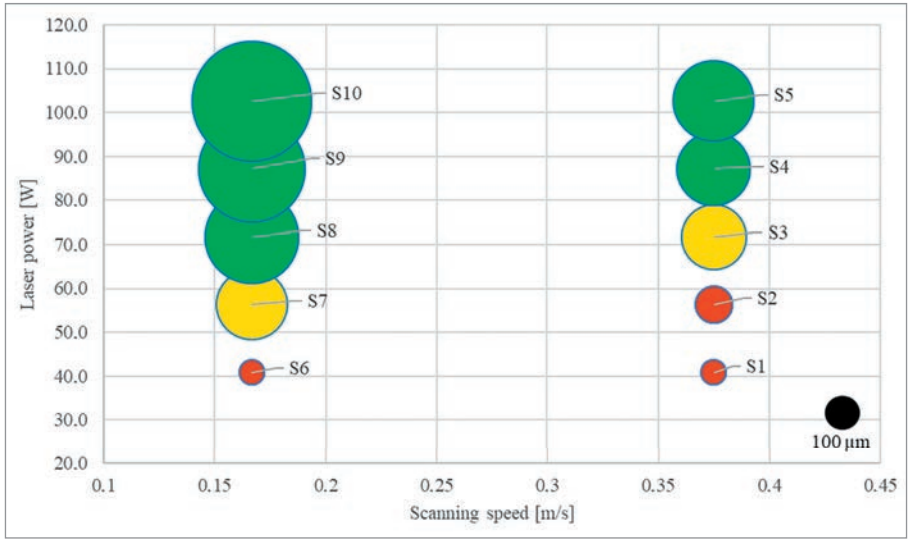

Figure 13 *TEST3 parameters and results*

TEST4 explored the regions of higher laser power and scanning speeds to some extent (Figure 14). Despite increased beam energy, the tracks' thickness did not increase significantly, likely due to a slightly higher laser speed that contributed to maintaining the energy density at a nearly constant level. Energy density for each track was calculated as explained by Fischer et al.[9] This trial provided some acceptable quality tracks, but fewer in number and still thick in width (S1, S3, S9).

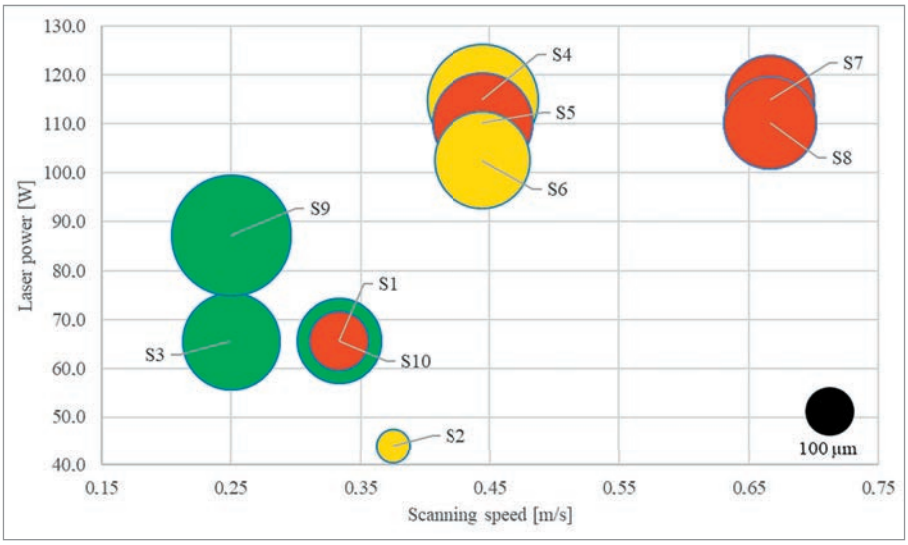

Figure 14 *TEST4 parameters and results*

In contrast, TEST5 spanned the region of low scanning speeds (0.075–0.19 m/s) and relatively lower laser power (Figure 15). A relevant number of sharp tracks were obtained (thickness 70–106 µm) but were endowed with remarkable balling defects, melt instability and gaps. Only three stable tracks were revealed, but they were still too thick (S8, S9, S10). These large and stable vectors are not suitable for resolution improvement but can be of certain utility as hatch vectors for bulk printing.

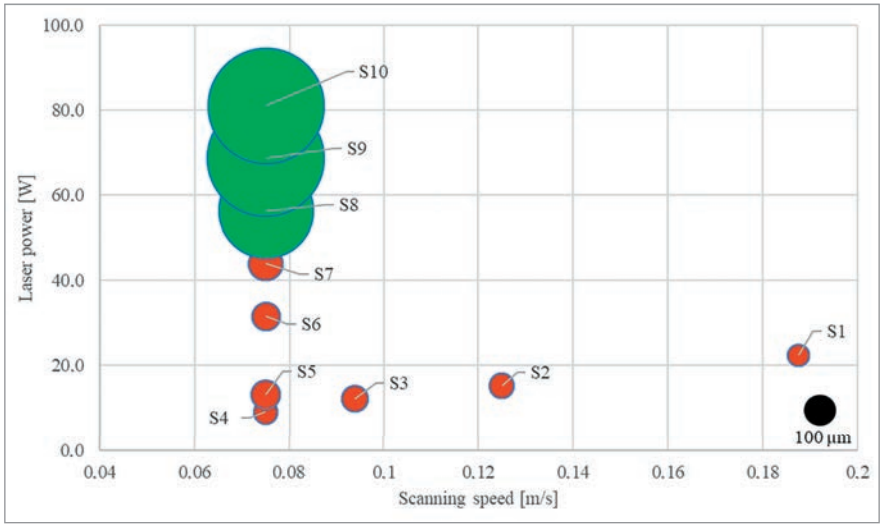

Figure 15 *TEST5 parameters and results*

After analyzing the results of these initial printing tests, it was determined that the best thin vector is S11 from TEST2; it resulted in an intermediate quality and stability combined with an acceptably low thickness (89 µm). For this vector, laser power was 44 W and scanning speed was 0.375 m/s (i.e., exposure time of 40 µs and spot distance of 15 µm). These laser parameters were used for the outer vector in the successive tests with layer 30 µm and powder 0–25 µm. In Figure 16, the S11 vector from TEST2 is shown. It must be noted that the first and last tracks (i.e., the most right and the most left) were printed with different parameters because they act as "reinforcement" for the contained tracks and are not part of the investigation. This expedient was necessary since the thinner vectors were easily broken during handling after printing.

Figure 16 *Vector S11 with 44 W and 0.375 m/s from TEST2*

Further vector tests were printed in order to find thinner and more stable vectors, but vector S11 from TEST2 still provided the best result.

In TEST6, a couple of identical boxes (BOX1, BOX2) were printed by selecting the best track quality from the preceding trials and suitable hatching strategy. The only difference was the presence or absence of the outer scan. This difference aimed to study the effect of the outer scan on the exterior quality of printed items. The parameters for contouring fill lines were power 65.5 W and scanning speed 0.33 m/s (S5, TEST1). Hatches had power of 87.1 W and scanning speed of 0.167 m/s (S9, TEST3). As previously stated, the overlapping rate for both fill lines and hatches was 75%. For example, the above-mentioned fill-line tracks are 200 µm thick, so the shifting between subsequent fill-lines laser scan is 200 µm x (1 – 75%) = 200 µm x 0.25 = 50 µm. Beam compensation for boxes of TEST6 was 0.07 mm. For all samples, scanning strategy printed from the outside to inside: outer first, then fill lines and hatches last.

It is evident that application of an outer laser scan to improve the detail resolution led to a deleterious increase in roughness (Figure 17). Instead, without the outer scan, the box surface appears significantly smoother (Figure 18) though not perfect because of partial balling phenomenon. The higher roughness of resolution sample (RS) with outer scan (RS1) is also evident on the star side walls (Figure 19), blades (Figure 20) and slots (Figure 21). On the other hand, the presence of an outer scan allows to obtain more specific details of resolution samples. This can be confirmed by both the presence of numbers (Figure 22) and the almost complete blades present from the initial to the penultimate set (0.1 mm), which are missing in RS2 of the same test.

Figure 17 *BOX1 (TEST6) after metallographic section*

Figure 18 *BOX2 (TEST6) after metallographic section*

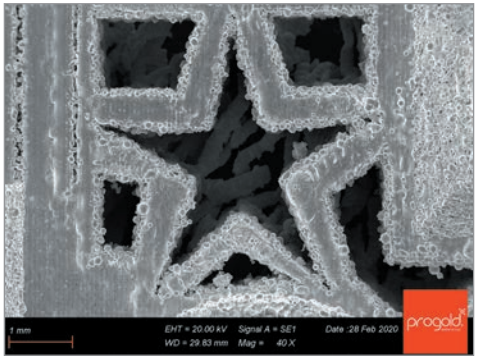

Figure 19 *Star walls—detail of resolution sample (RS1) with outer scan (TEST6)*

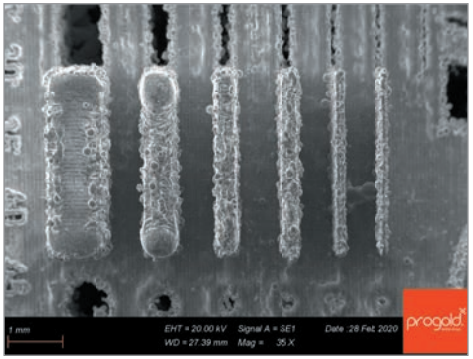

Figure 20 *Blades—top detail of resolution sample (RS1) with outer scan (TEST6)*

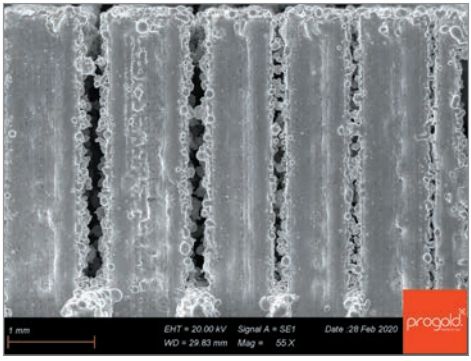

Figure 21 *Slots—detail of resolution sample (RS1) with outer scan (TEST6)*

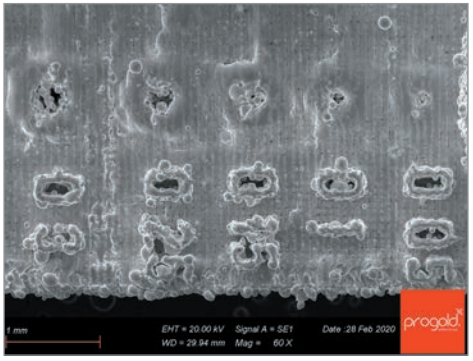

Figure 22 *Numbers and holes—detail of resolution sample (RS1) with outer scan (TEST6)*

In the case of resolution samples without an outer scan, the edges are acceptably smooth as with the box sample (Figures 23–25). While the slots are cleaner, the blades are missing the three thinnest ones (Figure 24), and the details for the numbers are completely absent (Figure 26).

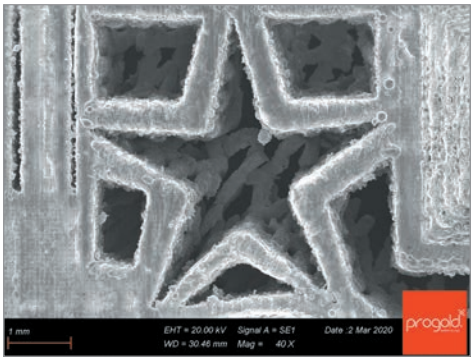

Figure 23 *Star walls—detail of resolution sample (RS2) without outer scan (TEST6)*

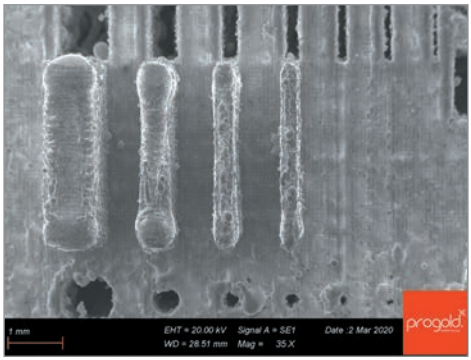

Figure 24 *Blades—detail of resolution sample (RS2) with outer scan (TEST6)*

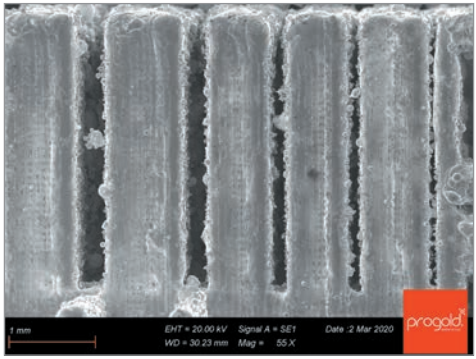

Figure 25 *Slots—detail of resolution sample (RS2) with outer scan (TEST6)*

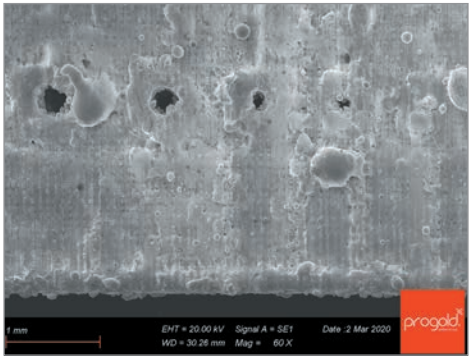

Figure 26 *Missing numbers and holes—detail of resolution sample (RS2) without outer scan (TEST6)*

TEST7 was the final printing test for 0–25 µm powder and 30 µm layer. In this test, a couple of boxes and resolution samples were printed. RS2 proved to be the best strategy. We used three thin fill lines as outer vectors with 0.02 mm of distance between the first and the following ones, and ten thicker fill lines between outer vectors and hatches. Double scanning strategy for hatches was adopted, with a hatch offset (i.e., distance from boundaries) of 0.35 mm. It was demonstrated by Zito et al. that double scanning leads to higher final density (i.e., less residual porosity in parts).[2] Table 2 summarizes all the printing parameters and conditions for RS2, TEST7. Figures 27–30 show the printing details of RS2 in TEST7.

Table 2 RS2 final strategy for 30 µm layer and 0–25 µm powder (TEST7)

SAMPLE	OUTER	FILL LINE			HATCH		
	LASER	LASER	NUMBER [N]	DISTANCE [mm]	LASER	DISTANCE [mm]	OFFSET [mm]
SR2	TEST-S11	TEST1-S5	10	0.05	TEST-S9	0.083	0.35

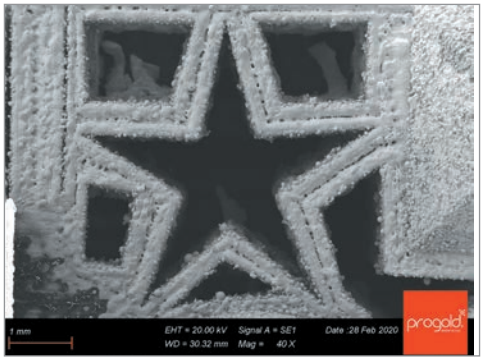

***Figure** 27 Star walls—detail of resolution sample (RS2) from TEST7*

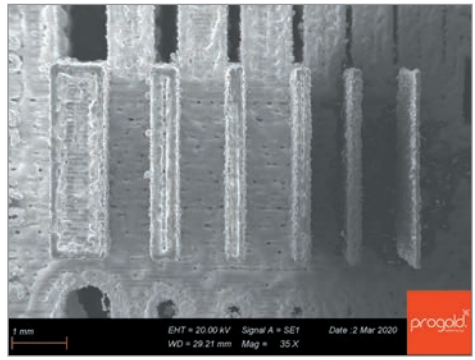

***Figure 28** Blades—top detail of resolution sample (RS2) from TEST7*

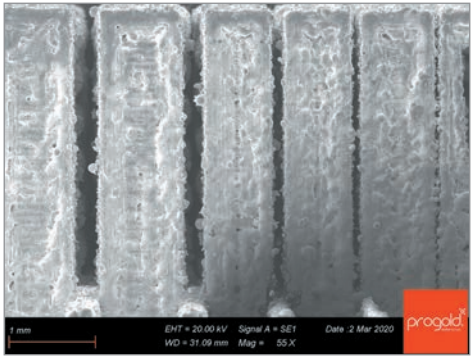

***Figure 29** Slots—detail of resolution sample (RS2) from TEST7*

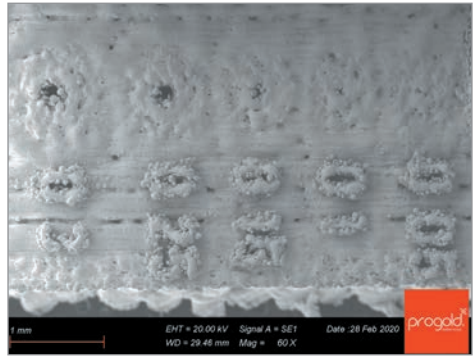

***Figure 30** Holes and numbers—detail of resolution sample (RS2) from TEST7*

TEST8 was carried out to evaluate the thickness of the laser melting tracks by using a powder size of 0–15 µm and printing layer of 30 µm. Laser power was from about 20 W up to approximately 100 W, and the scanning speed was shifted from 0.075 m/s up to 0.375 m/s with nearly 0.100 m/s stepwise (Figure 31). In almost all cases, laser power higher than 80 W gave nice and straight vector tracks, but their thickness was greater than our reference value and thus cannot be considered suitable for increased resolution. The general trend under 60 W showed sharp tracks thinner than the reference value but discontinuous (with gaps) and rough to some extent. The discontinuity seems to depend on a commencement of the

balling effect that makes the melting pool more unstable. Only one exception—S18 at 60 W and quite high scanning speed (0.375 m/s)—showed a good quality and a 97 µm thickness. In order to discover better stability conditions for laser parameters, the parameters of the best sample S18 were slightly modified, varying laser power and scanning speed to look for improvements (Figures 32). In Figure 33, the S18_8 sample gave the best result from refinement of TEST8—S18. This sample was 89 µm thick so it was used as an outer vector for further box and resolution sample tests.

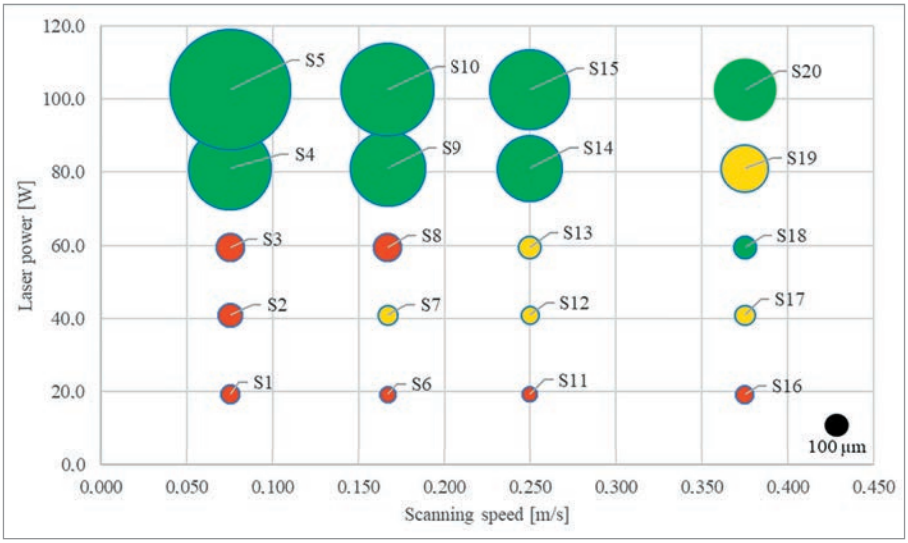

Figure 31 *TEST8 parameters and results*

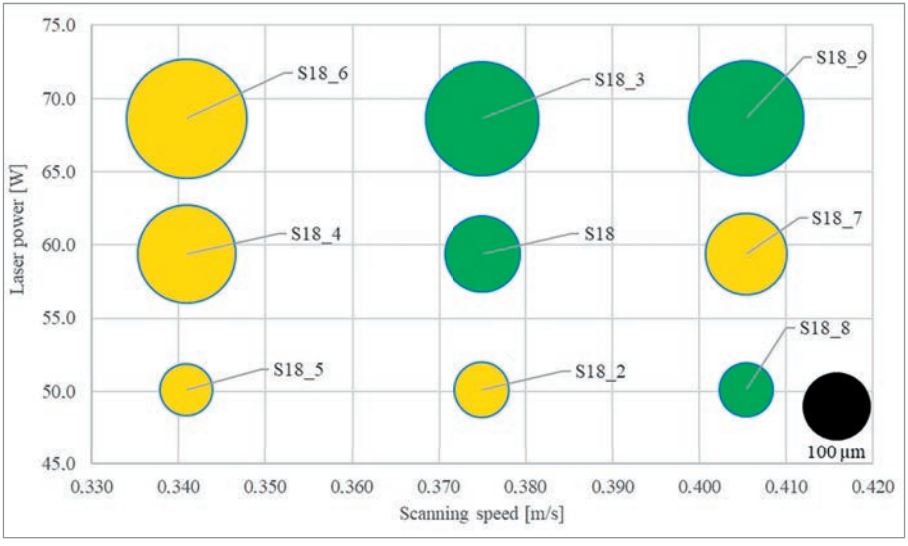

Figure 32 *The refinements around the best result of TEST8 (S18): 30 µm layer, powder 0–15 µm*

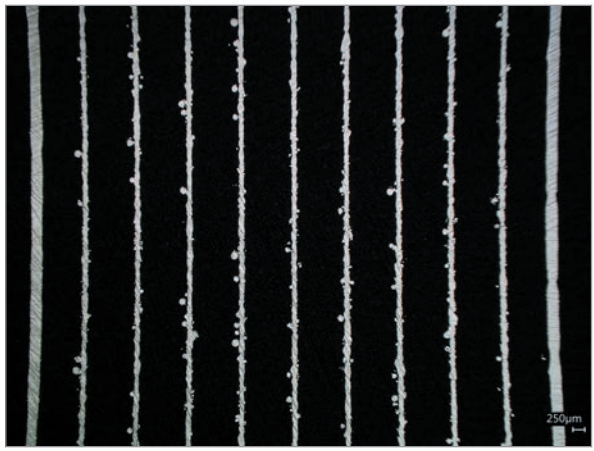

Figure 33 *S18_8 vector tracks from refinement of TEST8—S18*

In following trials, we printed other vectors to look for thicker and more stable tracks to be used as fill lines and hatches. Thus, in TEST9, we printed several boxes and resolution samples. The resulting best ones were BOX1 and RS1, printed with identical parameters. For these samples, the fill lines were printed using a track with a medium thickness (154 µm) and good track stability with a laser power of nearly 70 W and scanning speed of 0.375 m/s. The inner hatches (270 µm) were scanned at higher laser power (81 W) and lower scanning speed (0.167 m/s) in order to obtain a faster growth and better joining between tracks (Figure 34). The RS1 parameters are summarized in Table 3.

An interesting result emerged from another resolution sample printed during TEST9: RS2. The only difference between the RS1 and RS2 of TEST9 was the order of outer vector printing. For RS1, the outer was printed before fill lines and hatches, while the outer of RS2 was printed after fill lines and hatches. Resulting surfaces of RS1 were better than those of RS2, and this allowed us to understand that if the outer vectors are printed before the fill lines, the smoothness of printed parts will be better. This phenomenon can be explained by taking into account that the outer vectors are completely re-melted by the neighboring thicker fill line. Through re-melting the outer contour, the surface will take the side roughness of the last vector that is scanned (i.e., fill line in RS1). The hatches are usually scanned after outer and fill-line vectors, but they do not affect surface quality since they have a consistent distance from the slice contour boundary: the hatch offset. With RS2, the scanned outer did not have enough laser energy to completely re-melt the already consolidated fill lines since they are massive compared to the thinner outer vectors. The laser energy of outer vector is transferred to the fill-line wall and the generated heat promotes the phenomenon of particles sticking on the external surface. Thus, surface roughness is increased.

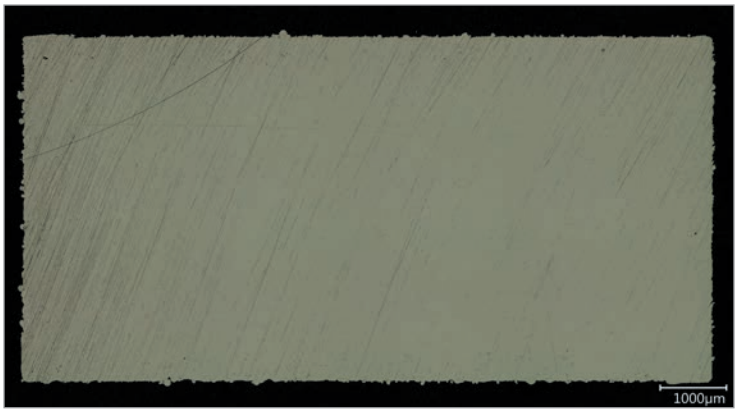

Figure 34 *The smoothest box (BOX1) with the best outer track (S18_8) from TEST9*

Table 3 *RS1 final strategy for 30 µm layer and 0–15 µm powder (TEST9)*

SAMPLE	OUTER	FILL LINE			HATCH		
	LASER	LASER	NUMBER [N]	DISTANCE [mm]	LASER	DISTANCE [mm]	OFFSET [mm]
RS1	TEST8 - S18_8	TEST14 - S2	10	0.046	TEST14 - S4	0.077	0.3

The printing conditions of the first box and resolution sample (TEST9) led to a resolution sample showing slightly better edge sharpness, cleaner surfaces and improved definition of numbers (Figures 35–38). The blades appeared significantly freer from attached particles than most of the resolution samples obtained with coarser powder (0–25 µm). The same applies for slot undercuts and number details.

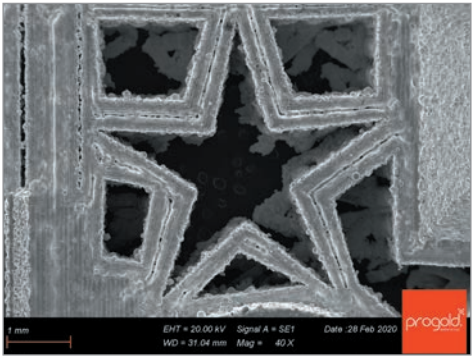

Figure 35 *Star walls—detail of resolution sample (RS1) from TEST9*

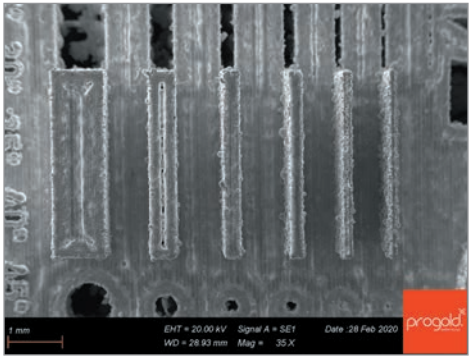

Figure 36 *Blades—top detail of resolution sample (RS1) from TEST9*

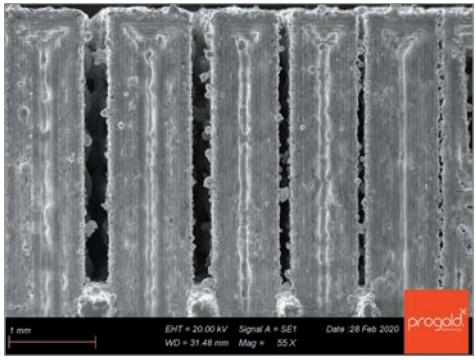

Figure 37 *Slots—detail of resolution sample (RS1) from TEST9*

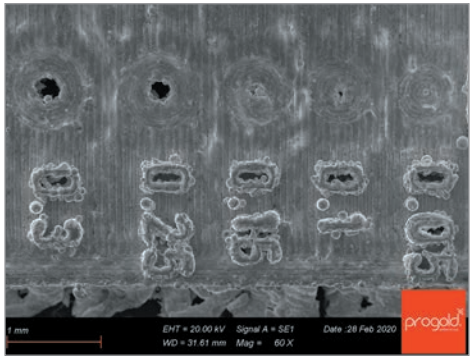

Figure 38 *Holes and numbers—detail of resolution sample (RS1) from TEST9*

TEST10 was printed with a layer thickness of 20 µm and generally lower laser power in order to avoid over-melting of the thinner powder bed. Laser power ranged from about 13 W to approximately 80 W with a step of nearly 20 W. The scanning speed variation was the same as in the previous trials (Figure 39).

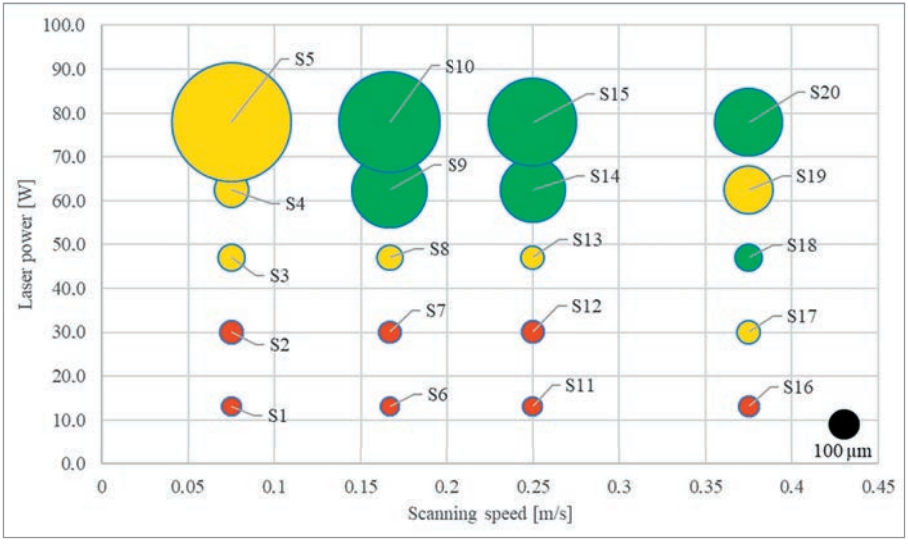

Figure 39 *TEST10 parameters and results*

A further refinement of the range of printing parameters was carried out by taking the best vector of TEST10 (S18) plus another one not printed in TEST10 (S21_1) and applying small modifications in both laser power and scanning speed (Figure 40). The latter sample (S21_1 at 50 W and 0.333 m/s) was created during the refinement stage in order to cover a greater range in scanning speed

and laser power. From this refinement, two satisfactory vectors were obtained: the thickness for these two was 76 µm for the first one (S18_7) and 85 µm for the second (S21_7). Figure 41 shows the tracks of vector S18_7 that were used as outer vector for the following boxes and resolution sample tests.

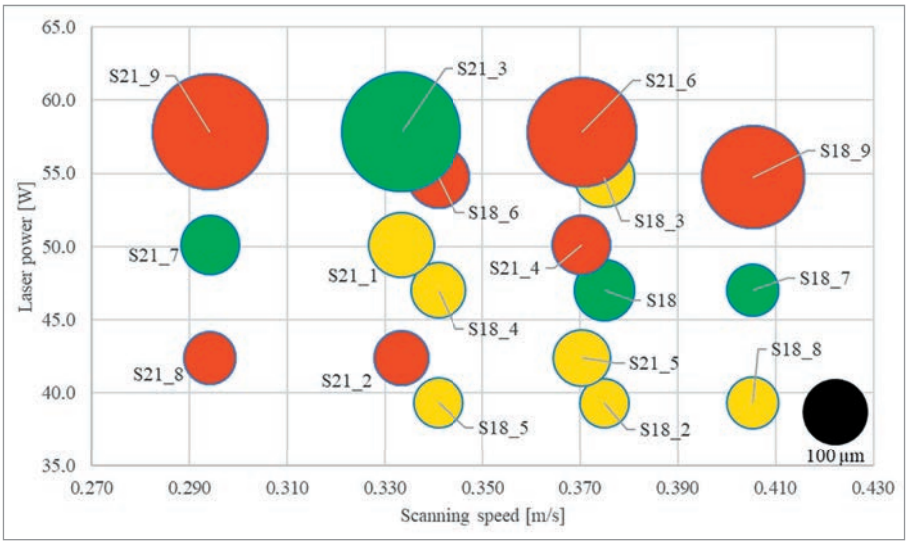

Figure 40 *The refinements around best result of TEST10 (S18) and S21_1 (20 µm layer, powder 0–15 µm)*

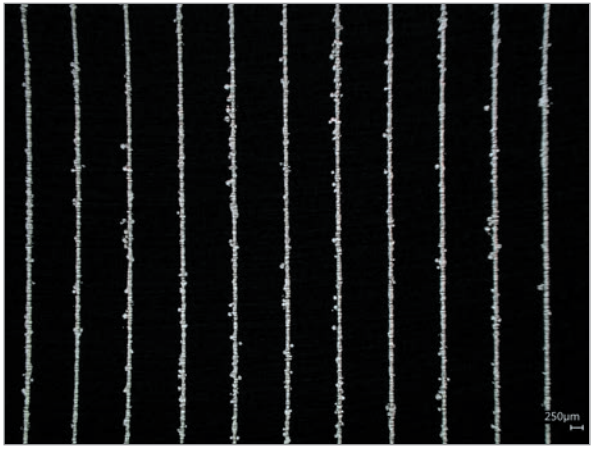

Figure 41 *S18_7 vector tracks from refinement of TEST10 – S18*

In the interest of printing the complete strategy, we selected vector S20 from TEST10 for fill-line parameters. Its tracks measured an average of 190 µm and it exhibited a very good stability. In the same manner, vector sample S15 from the same test was used for hatching. Its higher scanning energy led to a thickness of about 240 µm. The contour scanning in TEST11 (i.e., boxes and resolution samples test) was created using three thin fill lines as outer vector (these three fill lines have the outer vector parameters) as done in previous TEST7, with 0.016 mm of distance between them. In TEST11 we printed several boxes and resolution samples with different strategies, and this time, also, the best ones were BOX1 and RS1. Their parameters are listed in Table 4. The overlapping for all the tracks remained at 75%. The BOX1 and RS1 details are shown in Figures 42–46.

Table 4 *RS1 final strategy for 20 µm layer and 0–15 µm powder (TEST11)*

SAMPLE	OUTER	FILL LINE			HATCH		
	LASER	LASER	NUMBER [N]	DISTANCE [mm]	LASER	DISTANCE [mm]	OFFSET [mm]
RS1	TEST10 - S18_7	TEST10 - S20	9	0.048	TEST10 - S15	0.06	0.35

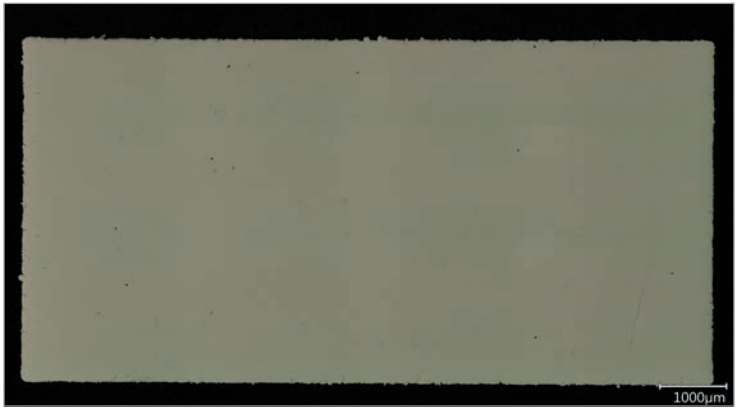

Figure 42 *The smoothest sample—BOX1—with S18_7 outer vectors from TEST11*

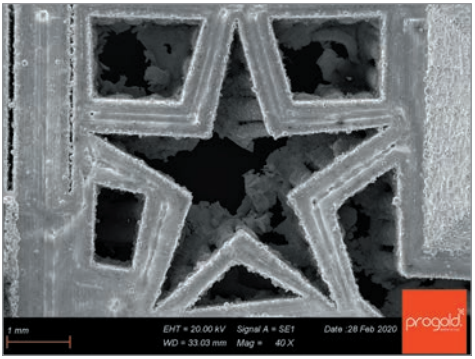

Figure 43 *Star walls—detail of resolution sample (RS1) from TEST11*

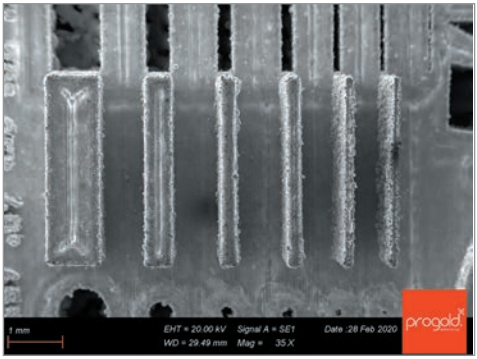

Figure 44 *Blades top—detail of resolution sample (RS1) from TEST11*

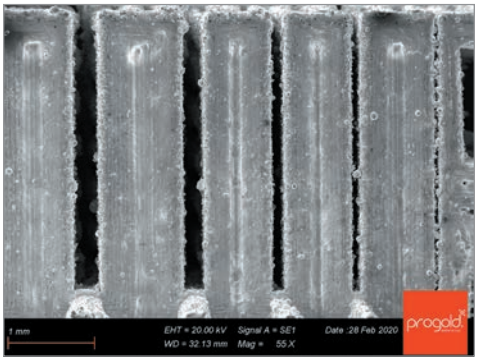

Figure 45 *Slots—detail of resolution sample (RS1) from TEST11*

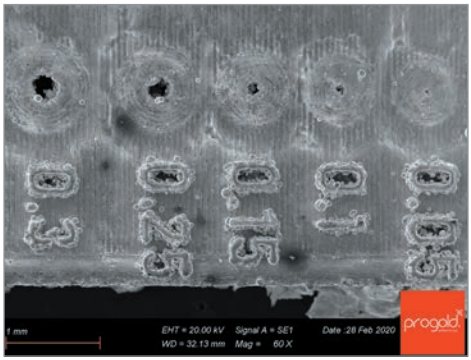

Figure 46 *Holes and numbers—detail of resolution sample (RS1) from TEST11*

TEST12 was performed with a building layer of only 15 µm and, consequently, lower laser power in order to avoid an excessive melting of the thinner powder bed. Laser power ranged from about 16 W to approximately 60 W with a step of nearly 10 W. The scanning speed variation was the same used in the previous trials (Figure 47). A further refinement of the printing parameters was carried out by taking the best two vectors of TEST12 (S14 and S19 in Figure 48). The best stability and smallest track thickness (70 µm) both resulted from sample S19_4 (Figure 49). Therefore, this condition was used in subsequent TEST13 for the three thin "outer" fill lines, with a distance of 0.021 mm between one track and the other.

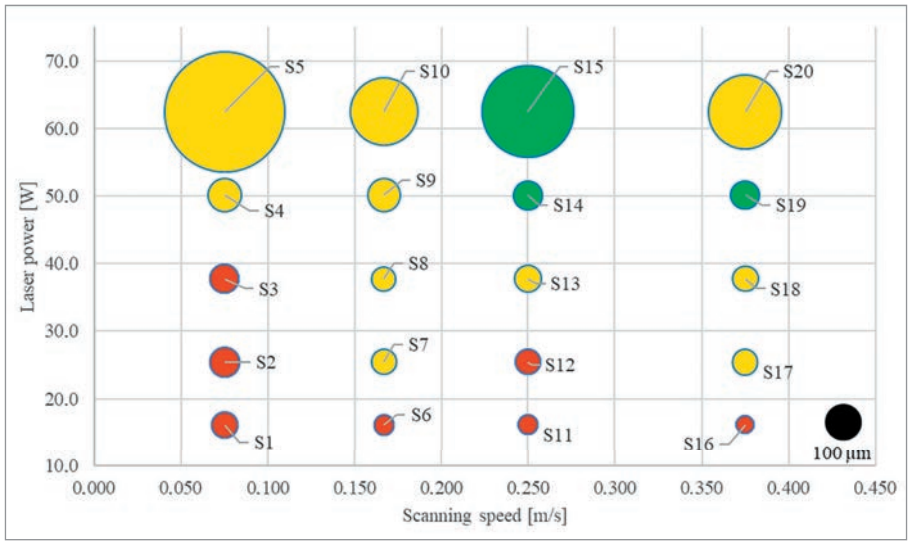

Figure 47 *TEST12 parameters and results*

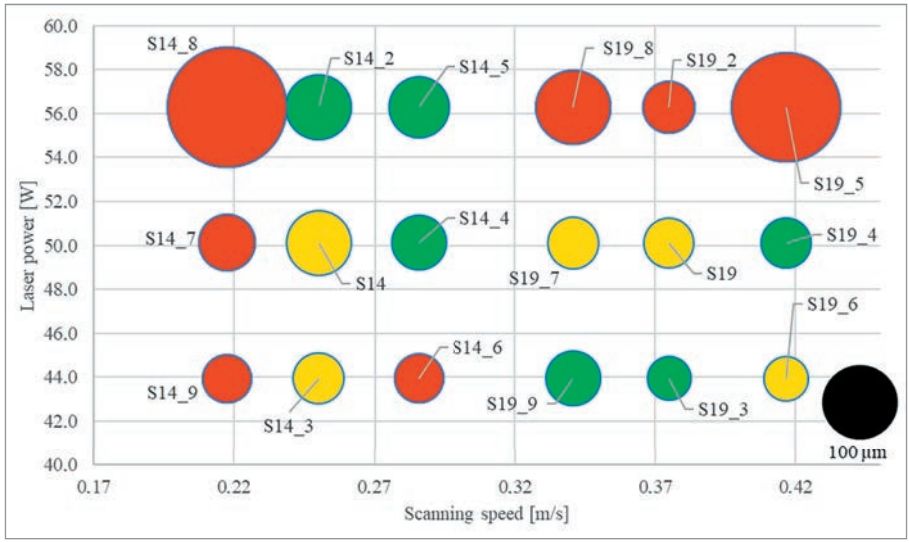

Figure 48 *The refinements around best results of TEST12 (S14, S19)—15 µm layer, powder 0–15 µm*

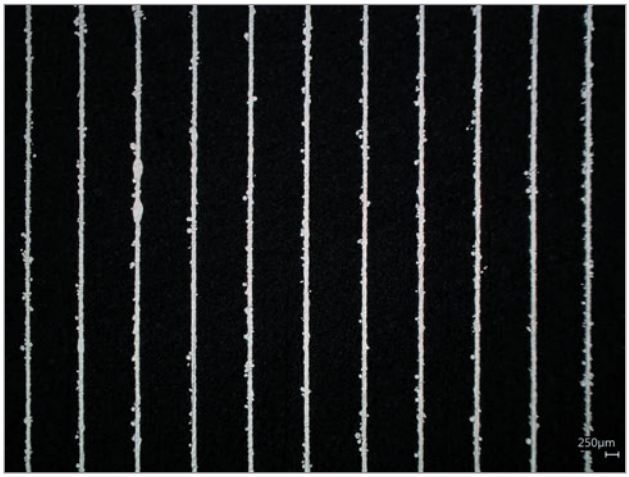

Figure 49 *S19_4 vector tracks from refinement of TEST12 – S19*

To print boxes and resolution samples in TEST13, the vector S15 of TEST12, which showed high stability and 210 µm of thickness, was used for both fill lines and hatches. Table 5 repeats the strategy adopted to print RS1 (and BOX1) that yields the best results for this layer thickness and powder granulometry.

Table 5 *RS1 final strategy for 15 µm layer and 0–15 µm powder (TEST13)*

SAMPLE	OUTER	FILL LINE			HATCH		
	LASER	LASER	NUMBER [N]	DISTANCE [mm]	LASER	DISTANCE [mm]	OFFSET [mm]
RS1	TEST12 - S19_4	TEST12 - S15	9	0.052	TEST12 - S15	0.052	0.35

BOX1 in Figure 50 shows that the same scanning strategy adopted for thicker building layers does not work very well for this thinner one. Rows of small pores are visible under the outer shell of the box sample. It is probable that the overlapping (but probably also other parameters) should be adapted for this layer thickness. To investigate this phenomenon, further tests are required but were not considered in the current research work. RS1 details are shown in Figures 51–54.

Figure 50 *The sample BOX1 of TEST13 shows some internal porosity.*

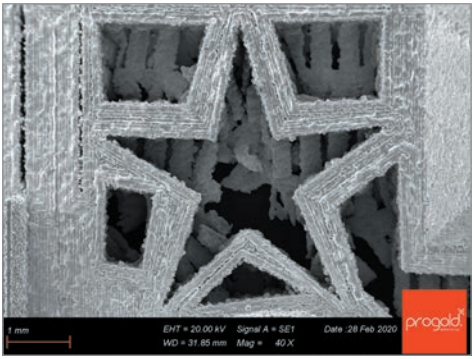

Figure 51 *Star walls—detail of resolution sample (RS1) from TEST13*

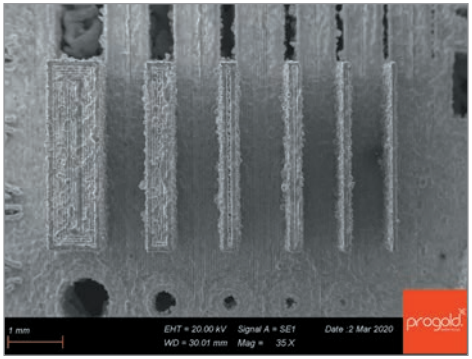

Figure 52 *Blades—top detail of resolution sample (RS1) from TEST13*

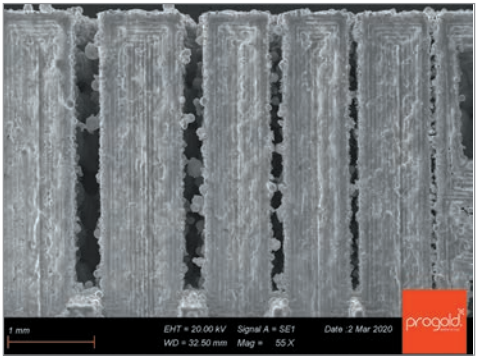

Figure 53 *Slots—detail of resolution sample (RS1) from TEST13*

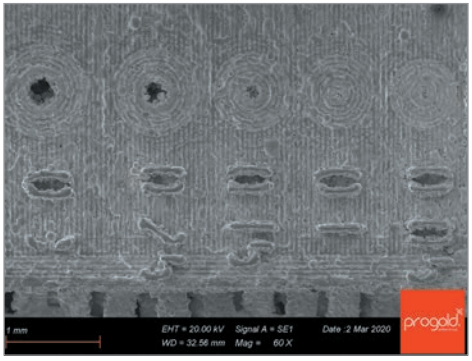

Figure 54 *Holes and numbers—detail of resolution sample (RS1) from TEST13*

In order to appreciate the improvements of the tests results, the quality starting point of the resolution sample made with standard laser parameters is reported for comparison. In this case, "standard" laser parameter means the actual parameters used for production in our company for a powder with the same chemical composition, particle size of 15–53 µm and 30 µm layers. The outer vector was performed with a laser power of 76.2 W, exposure time of 40 µs and spot distance of 10 µm; the resulting scanning speed was 0.25 m/s. These parameters result in a vector about 240 µm thick, which is considerably larger than the outer vectors used in this research. The hatch laser parameters were as follows: laser power at about 70.6 W, exposure time of 40 µs and spot distance of 20 µm (i.e., scanning speed of 0.5 m/s), giving a track about 180 µm thick. Hatch distance was 0.09 mm—this means an overlapping rate of nearly 50%. Beam compensation was 0.22 mm. In standard scanning strategy, no fill lines were planned.

In the case of the star module, the standard resolution sample clearly suffered from remarkable grooves on the surface that gave an irregular appearance (Figure 55), while star details obtained during this last research typically showed smoother surfaces and cleaner edges (Figures 23 and 43), with the exception of a few trials (Figures 19 and 51).

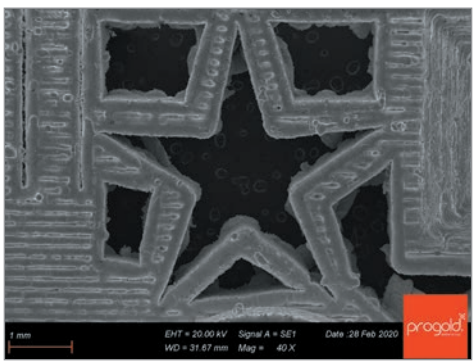

Figure 55 *Star—detail of standard resolution sample*

The blade module in standard resolution sample was missing the three thinner blades (Figure 56), while in the resolution samples printed for this research, the entire group of blades was always present up to the penultimate one (0.10 mm; no sample presents the thinnest 0.05 mm blade). The only exception is the sample built with coarser powder (0–25 µm) and thicker layer of 30 µm (Figure 24).

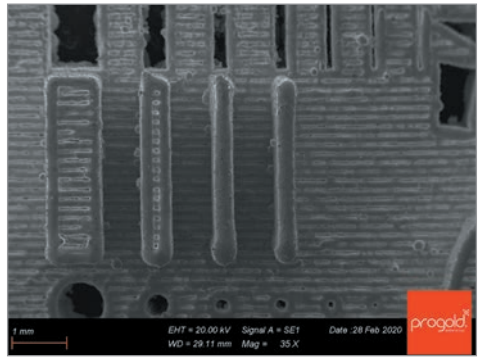

Figure 56 *Blades—detail of standard resolution sample*

The slots area of the standard resolution sample was of medium quality, but the inner sides of the undercuts contained a lot of glued on particles and fins. The slots under 0.20 mm width appeared to be choked by much unmelted debris, and the presence of a deeply grooved surface made them appear much more unattractive (Figure 57).

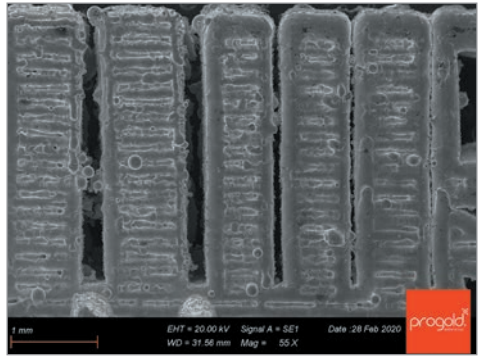

Figure 57 *Slots—detail for resolution sample with standard laser parameters*

The numbers detail of the standard resolution sample show that very thin details cannot be obtained with that printing strategy (Figure 58). At this point, the relevant difference between standard and refined printing conditions is clear. Especially for the printed numbers, the standard strategy did not produce any digits, whereas the strategies of this study provided quite definite characters (Figures 22, 38 and 46).

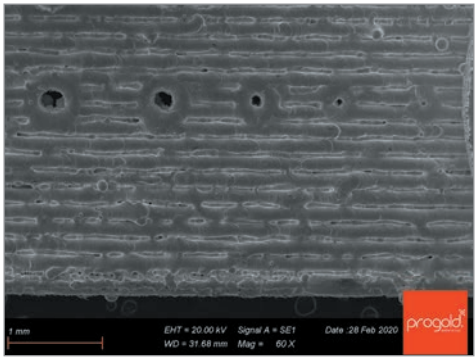

Figure 58 *Irregular holes and missing numbers—detail of standard resolution sample*

An additional quality check was made by measuring the roughness of the best samples obtained so far and comparing them with a specimen printed with the current standard laser parameter strategy. The measurement was carried out on a simple prismatic specimen arranged in two different ways on the building table. The first sample was arranged vertically (positioning the smaller face on the platform), which allows for roughness measurement along the Z-axis, and the second sample horizontally (i.e., with the wider face lying on platform) for roughness measurement along the X-axis of the printing process. In this research, the hatches were printed always in Y-axis direction, so the roughness was measured perpendicularly to the hatches. Figure 59 shows an example.

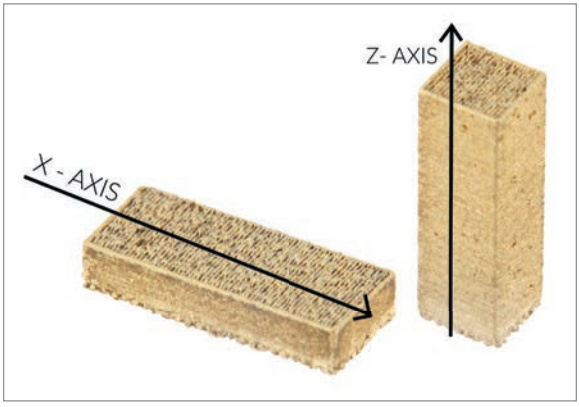

Figure 59 *Example of roughness measurement directions*

Three measurements were made for each direction and each sample. In Figure 60, the results are the average of three values. The roughness value considered is R_t (i.e., total roughness), which is the difference in height between the maximum peak and the minimum valley. This parameter is representative of a real concern

in jewelry manufacturing, since jewelry polishing must be continued until all the valleys are removed from the surface. It is worth mentioning that in the case of the standard printing process, the horizontal roughness is clearly higher than vertical roughness because of the presence of the deep grooves on the surface, while the high-resolution specimens provided an additional advantage, reversing this phenomenon: the horizontal roughness is lower than the vertical one.

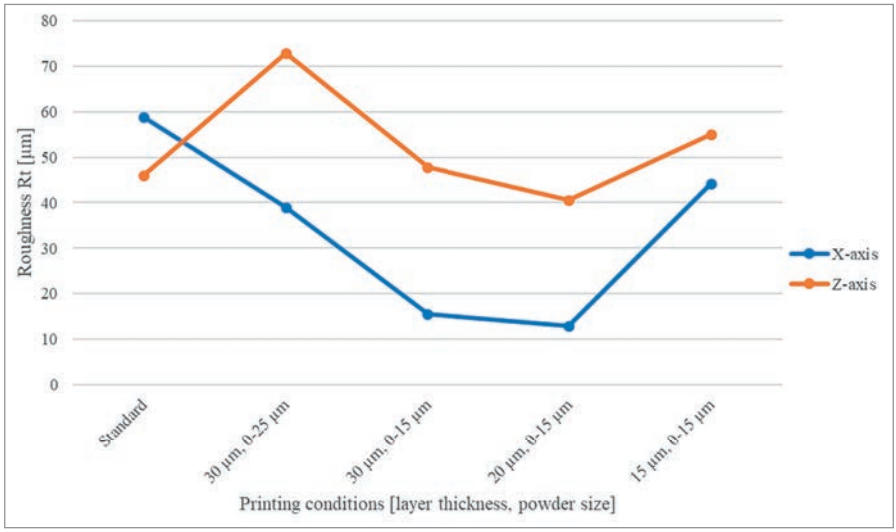

Figure 60 *Roughness measurement for each printing condition and standard strategy specimens*

Figures 61 and 62 show a complete comparison of the four printing conditions (different layer thickness and powder size) plus the standard strategy (on the right). The two selected details are the star and hole/number coupling since they are the two most representative to compare the improvements obtained in this research work.

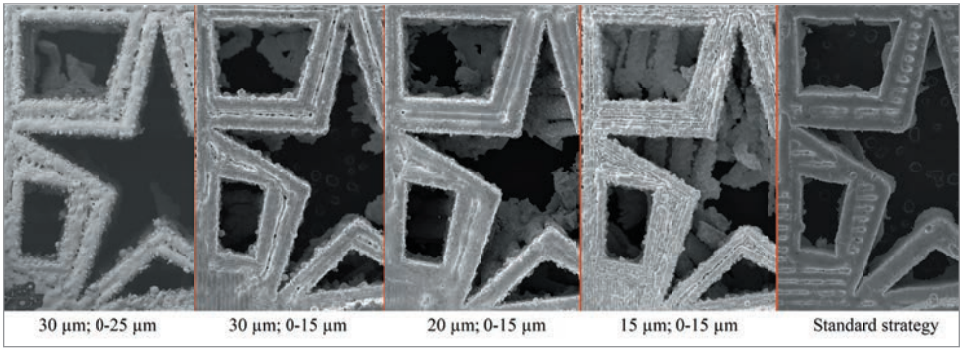

Figure 61 *Star—detail comparison (layer thickness; powder size)*

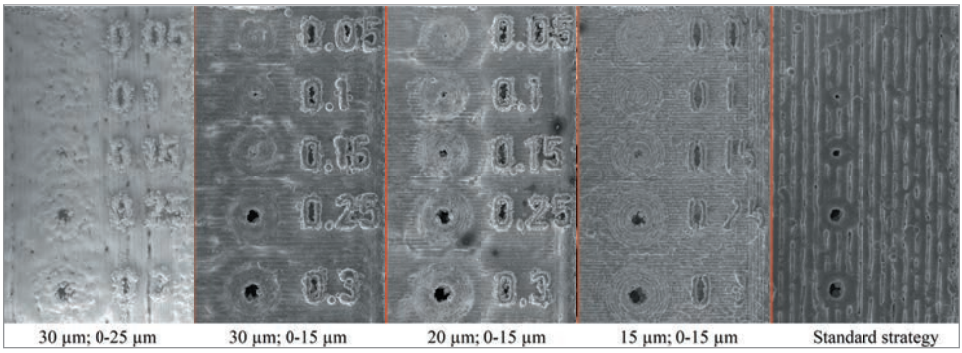

Figure 62 *Comparison of holes and numbers (layer thickness; powder size)*

To get a better visualization of the difference between the standard printing conditions and the improved strategies discovered in this research, and to transfer them into the world of jewelry manufacturing, a real ring design was printed (Figure 63). This ring was printed with standard printing strategy and with the best strategy determined among all the trials: TEST11 – RS1 (i.e., 20 µm layer and 0–15 µm powder). The selection of the best result in this research was based on detail coherence between physical samples and digital file (resolution sample details), internal residual porosity (visual estimation based on box section) and surface aesthetic aspect (surface roughness). As can be observed from the image on the right in Figure 63, one side of the ring was designed specifically to evaluate the ability of a printing strategy to reproduce the file details on real parts.

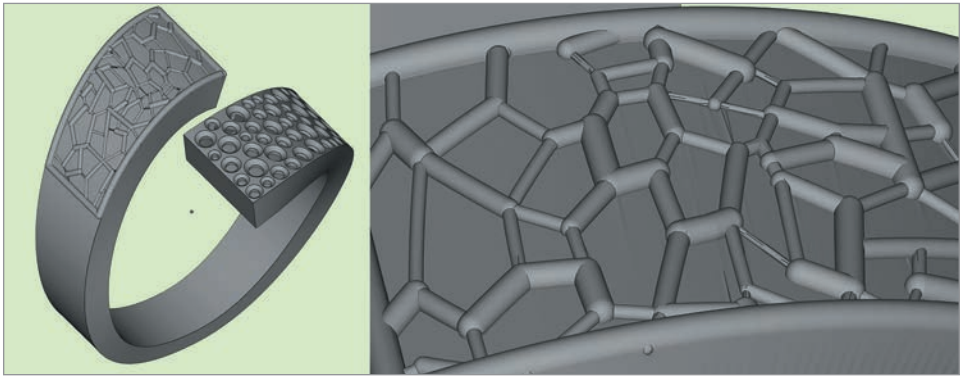

Figure 63 *Left: ring design made to compare the research improvements; right: thin details zoom*

Regarding the standard printing strategy, it was expected to find some missing details, just as happened when the corresponding resolution sample was printed. For this ring, the aesthetic aspect is very good since the surface is smooth and shiny after printing.

The ring printed using parameters from TEST11 – RS1 shows better detail reproduction. The general conformance to the file geometries is very high. Corners, edges and the sloping boundaries of holes are well defined and noticeable. The surface aspect, on the other hand, is not so shiny since some particles stick to the surface. As discerned from the printing test conducted, this phenomenon is due to a natural irregularity of tracks with thickness below the target 100 µm. These cannot be as smooth as a thicker trace (i.e., >150 µm). In Figure 64 a comparison is presented from the top view of the model.

Figure 64 *Left: standard strategy ring; right: best strategy ring*

Figures 65 and 66 show the comparison of the pavé side and the thin geometric details of the above-mentioned rings.

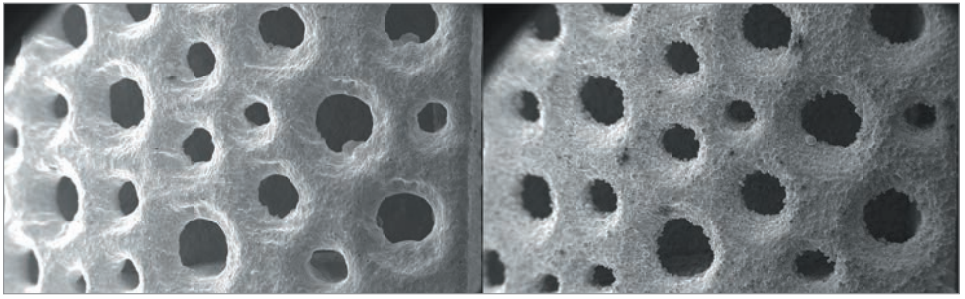

Figure 65 *Left: Pavé details of standard strategy ring; right: pavé details of best strategy ring*

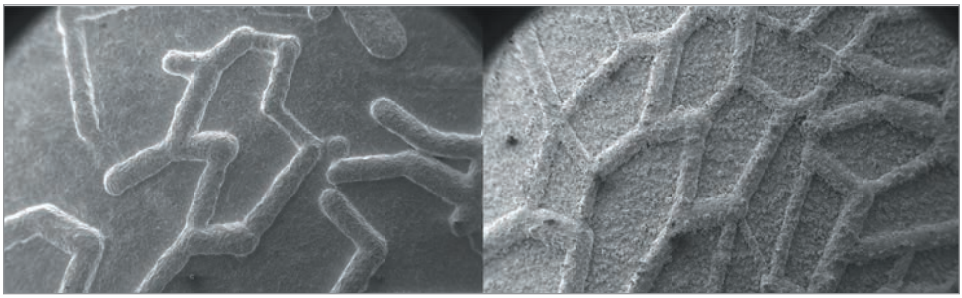

Figure 66 *Left: geometric details of standard strategy ring; right: geometric details of best strategy ring*

The last trial to evaluate the general performance of the high-resolution process consisted of printing ring sets that are typically manufactured by selective laser melting. Both scanning strategies (standard and high-resolution) were used. Thus, five different models were selected and printed. A computer rendering of the printed models is shown in Figure 67. At first sight, the comparison between low- and high-resolution processes reveals a slightly darker color for items printed using high resolution. As previously explained, this feature can be attributed in part to the higher quantity of agglomerated particles on the surface, which enhances the scattering of light. It is also evident that there is better definition of decorative details with the high-resolution process.

Figure 67 *Computer rendering of other models printed with both standard and best strategy*

A deeper analysis performed using optical microscopy revealed a very different appearance between the standard printing strategy, now qualifiable as low-resolution strategy, and the novel high-resolution strategy. For instance, the flower-lined ring shows the complete array of petals and stigmas when printed with high-resolution strategy while the total absence of those elements is evident in the ring printed with low-resolution strategy (Figure 68).

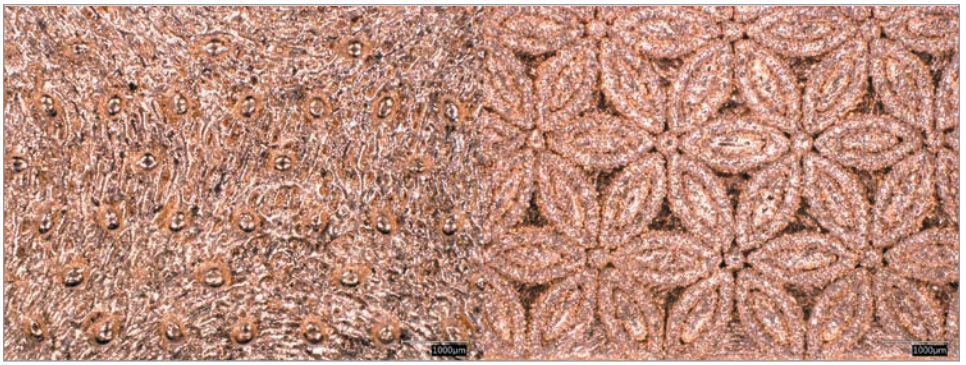

Figure 68 *Comparison of flower details with low- (left) and high-resolution strategy (right)*

The comparison between the bubble rings printed with low- and high-resolution processes (Figure 69, left and right, respectively) further highlights that the latter undoubtedly has a better surface quality. Furthermore, the surface roughness attained is much better for the high-resolution ring. The intersections between the bubbles are also trimmed by narrow and continuous curves, giving a more impressive definition of the spherical units.

Figure 69 *Comparison of bubble details with low- (left) and high-resolution strategy (right)*

The CAD image of the ferrules ring in Figure 70 shows blind holes coming up from the bottom. This design was purposely chosen to demonstrate the ability of the high-resolution strategy to reproduce difficult details. In Figure 71 (left) we can see that the low-resolution strategy is unable to print the hole caps, which are only 70 um thick. In Figure 71 (right) we can see that the high-resolution strategy nicely caps the holes, making them blind.

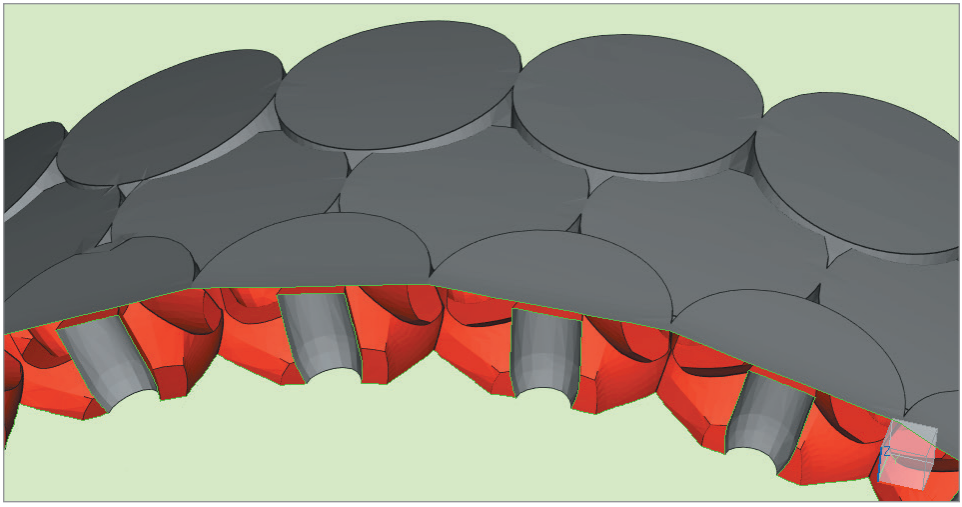

Figure 70 *A digital section of the ferrules ring*

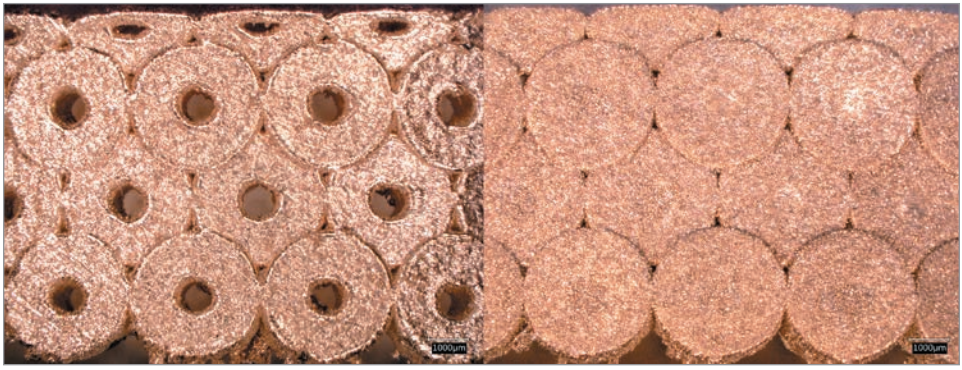

Figure 71 *Comparison of ferrule details with low- (left) and high-resolution strategy (right)*

The last real examples of high-resolution refinements attainable by using selective laser melting are displayed with the infinity ring (Figure 72) and fly-eye ring (Figure 73). It is clear that the dividing lines between the two halves of the infinity symbol are more marked in the high-resolution ring. The same applies for the plane edges. The taller building layer also causes higher total roughness and undulations, but this greater layer height is dictated by larger particle size (15–53 µm) in the low-resolution process. In the last comparison, the hexagons of the fly-eye are more defined and smoother and the hexagonal channels are more demarcated.

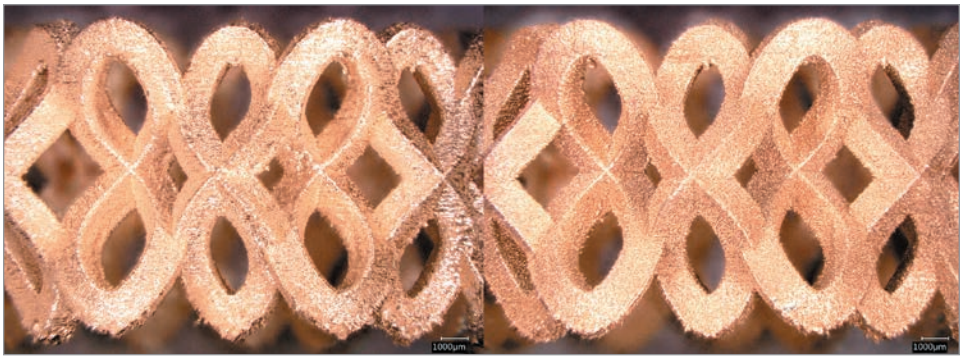

Figure 72 *Comparison of infinity ring details with low- (left) and high-resolution strategy (right)*

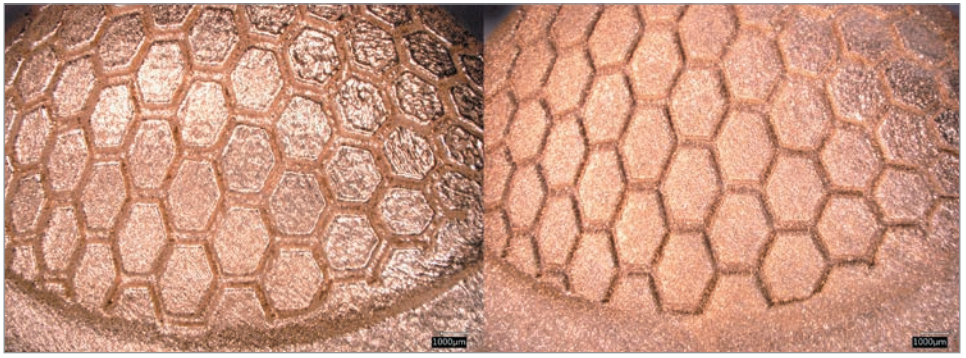

Figure 73 *Comparison of fly-eye details with low- (left) and high-resolution strategy (right)*

Conclusions

The goal of this research study was to increase the decorative detail resolution of jewelry items printed with SLM™ technique by tailoring the powder particle size, building layer height and laser scanning parameters. After an initial investigation on laser power and scanning speed parameters, we selected the parameters that allowed printing of a stable and narrow track, i.e., thinner than 100 µm. Amongst the spanned ranges of powder size and printing conditions, the best were attained with smaller particle size (0–15 µm) and intermediate layer thickness of vector sample S18_7 from TEST11 (20 µm). The analytical details of resolution sample (RS1) showed high conformance to plan geometry, clean and sharp edges and smooth surfaces (Figure 42–46). The narrow channels in the slots modules are fairly achievable almost up to the thinnest width (0.05 mm) and the blade relief up to the penultimate thickness (0.10 mm) without the phenomenon of heavy particles sticking.

In a similar way, the numeric fonts are almost perfectly executed into a continuous and uniform line, and hole walls are also reproduced to the smallest diameter (0.05 mm). There were some attached particles on the numbers and hole walls which may be removed by means of a suitable sand-blasting finishing process. The performance of the best printing parameters was tested by producing real jewelry items, and they provided a significant improvement with the rendering of the narrowest and sharpest decorative details.

It has been found that current standard printing strategy was not able to reproduce metal vectors thinner than about 300 µm, while the novel process can render thickness down to 100 µm. This advantage is likely responsible for the improvement of the edge definition and uniformity, as can be seen in pavé presetting areas (Figure 62) and in the substantial reduction of geometry collapses on the support sides. Further printings of real jewelry items validated that the newest building conditions can significantly improve the resolution of decorative details with selective laser melting.

References

1. Damiano Zito et al., "Latest Developments in Selective Laser Melting Production of Gold Jewelry," *The Santa Fe Symposium on Jewelry Manufacturing Technology 2012*, ed. E. Bell (Albuquerque: Met-Chem Research, 2012).
2. Damiano Zito et al., "Optimization of the Main Selective Laser Melting Technology Parameters in the Production of Precious Metal Jewelry," *The Santa Fe Symposium on Jewelry Manufacturing Technology 2013*, ed. E. Bell and J. Haldeman (Albuquerque: Met-Chem Research, 2013).
3. Damiano Zito et al., "Optimization of SLM Technology Main Parameters in the Production of Gold and Platinum Jewelry," *The Santa Fe Symposium on Jewelry Manufacturing Technology 2014*, ed. E. Bell and J. Haldeman (Albuquerque: Met-Chem Research, 2014).
4. Damiano Zito, "Use of gold powder alloys for manufacturing jewellery items by selective laser melting," WO Patent WO2015173790A1 (issued December 22, 2016).
5. Damiano Zito et al., "Definition and Solidity of Gold and Platinum Jewelry Produced Using Selective Laser Melting (SLM™) Technology," *The Santa Fe Symposium on Jewelry Manufacturing Technology 2015*, ed. E. Bell et al. (Albuquerque: Met-Chem Research, 2015).
6. Damiano Zito et al., "Potential and Innovation of Selective Laser Melting (SLM) Technique in Platinum Jewelry Production," *The Santa Fe Symposium on Jewelry Manufacturing Technology 2018*, ed. E. Bell et al. (Albuquerque: Met-Chem Research, 2018).
7. Damiano Zito et al., "Direct 3D Metal Printing: A Trip through New Opportunities and Innovative Alloys," *The Santa Fe Symposium on Jewelry Manufacturing Technology 2016*, ed. E. Bell et al. (Albuquerque: Met-Chem Research, 2016).

8. Damiano Zito et al., “Why Should We Direct 3D Print Jewelry? A Comparison between Two Thoughts: Today and Tomorrow,” *The Santa Fe Symposium on Jewelry Manufacturing Technology 2017*, ed. E. Bell et al. (Albuquerque: Met-Chem Research, 2017).

9. J. Fischer et al., “Micro Laser Melting: Analyses of Current Potentials and Restrictions for the Additive Manufacturing of Micro Structures,” *Proceedings of the 25th Annual International Solid Freeform Fabrication Symposium* (2014).

10. Su Xubin and Yongqiang Yang, "Research on track overlapping during Selective Laser Melting of powders," *Journal of Materials Processing Technology* 212, no. 10 (October 2012): 2074-2079.